ELSEVIER

Chemical Engineering Journal 140 (2008) 448–456

Chemical Engineering Journal

www.elsevier.com/locate/cej

Predicting axial pressure profile of a CFB

Afsin Gungor *

Department of Mechanical Engineering, Faculty of Engineering and Architecture, Nigde University, 51100 Nigde, Turkey

Received 19 June 2007; received in revised form 16 November 2007; accepted 19 November 2007

Abstract

The numerical simulation of CFBs is an important tool in the prediction of its flow behavior. Predicting the axial pressure profile is one of the major difficulties in modeling a CFB. A model using a Particle Based Approach (PBA) is developed to accurately predict the axial pressure profile in CFBs. The simulation model accounts for the axial and radial distribution of voidage and velocity of the gas and solid phases, and for the solids volume fraction and particle size distribution of the solid phase. The model results are compared with and validated against atmospheric cold CFB experimental literature data. Ranges of experimental data used in comparisons are as follows: bed diameter from 0.05 to 0.305 m, bed height between 5 and 15.45 m, mean particle diameter from 76 to 812 μm, particle density from 189 to 2600 kg/m^3, solid circulation fluxes from 10.03 to 489 kg/m^2 s and gas superficial velocities from 2.71 to 10.68 m/s. The computational results agreed reasonably well with the experimental data. Moreover, both experimental data and model predictions show that the pressure drop profile is affected by the solid circulation flux and superficial velocity values in the riser. The pressure drop increases along the acceleration region as solid circulation flux increases and superficial velocity decreases.

Keywords: Circulating fluidized bed; Hydrodynamic model; Pressure drop; Acceleration zone; Numerical simulation

1. Introduction

Circulating fluidized beds (CFBs) have found a wide range of applications in various industries and thus the hydrodynamics of CFBs have become a major concern of interest to provide a general understanding for the design and operation principles.

It is a well known fact that the pressure drop profile along the riser is strongly dependent on the gas–solid behavior. Many experimental and theoretical studies in the field of pressure profile in CFBs are available in the literature [1–16].

According to the axial solid volume concentration profile, the riser is axially divided into two different zones: The bottom zone and the upper zone. In contrast to the upper zone, only few studies deal with the flow structure in the bottom zone of a CFB. Svensson et al. [4] investigated the bottom zone in the Chalmers CFB boiler using pressure measurements. Rhodes et al. [5] found that the core–annulus structure of the upper zone is extended into the bottom zone. According to Schlichthaerle and Werther [7] study, a higher solids concentration at the wall and a lower concentration in the center of the riser were found. The comparison with the axial pressure profile indicates the presence of strong local acceleration effects in the bottom zone.

Numerous studies on CFB riser regimes are available in the literature [17–24]. The motion of solids in vertical gas/particle flow is very complex. According to Yerushalmi et al. [17], the transport velocity is defined as the velocity at which it is possible to carry all of the solids fed into the riser out again, and thus it is impossible to maintain a fluidized bed without continuous recycle of solids back into the fluid bed. This is the critical gas velocity defining the transition between turbulent and fast fluidization flow regimes. A qualitative fluidization map is initially proposed by Yerushalmi et al. [17] and, later completed by Van de Velden et al. [18]. The occurrence of both mixed flow, required in most gas/solid reactions, and plug flow, required for most catalytic gas phase reactions, is strongly dependent upon combined operational parameters of gas superficial velocity and solids circulation rate. The gas mixing mode is strongly affected by the operating conditions, however with a specific dominant mode within a specific (U_0, G) range. At high velocities (U_0 > approximately (U_{tr} + 1) m/s) and high solids circulation rate (G > approximately 200 kg/m^2 s) plug (dominant core) flow is achieved. Mixing occurs at lower G or lower U_0.

* Tel.: +90 505 504 49 02; fax: +90 212 245 07 95.
E-mail address: afsingungor@hotmail.com.

1385-8947/$ – see front matter © 2007 Elsevier B.V. All rights reserved.
doi:10.1016/j.cej.2007.11.023

Nomenclature

Ar	Archimedes number ($[d_p^3(\rho - C)Cg]/\mu^2$)
C	gas concentration (kg/m^3)
C_D	drag coefficient
d_p	mean particle diameter (m)
d_{pi}	particle dimension interval (m)
D	riser diameter (m)
D_b	bubble diameter (m)
g	gravity (m/s^2)
G	solids mass flux (kg/m^2 s)
$G(\varepsilon)$	solid stress modulus (N/m^2)
G_∞	the rate of elutriation above transfer disengaging height (kg/m^2 s)
h	height above the distributor (m)
h_{bot}	bottom zone height (m)
k_a	attrition constant
MW	molecular weight (kg/kmol)
P	pressure (kPa)
r	radial distance from riser axis (m)
R	riser radius (m)
R_u	universal gas constant (kJ/kmol K)
Re	Reynolds number
u	gas velocity (m/s)
u_b	bubble rise velocity (m/s)
U_0	superficial gas velocity (m/s)
U_{mf}	minimum fluidization velocity (m/s)
U_{tr}	transport velocity (m)
v	particle velocity (m/s)
x_a	weight fraction of particles after attrition in d_{pi} interval

Subscripts

mf	minimum fluidization
p	particle

Greek letters

α	decay coefficient
β	gas–solid friction coefficient
β'	constant defined in Eq. (8)
ε	void fraction
ε_b	bubble volume fraction
$\bar{\varepsilon}$	average void fraction
μ	viscosity (Pa s)
ρ	particle density (kg/m^3)
τ	shear stress (N/m^2)

When mixing occurs, the hydrodynamics of the riser can be modeled by a core/annulus approach [19]. In the mixing mode, a dilute region with rapidly rising particles exists in the core of the riser. This core is surrounded by a denser annulus of particles descending near the wall. In plug flow mode, most of the particles move upwards, and downward particles are randomly distributed across the section of the riser. At ambient conditions, reactors requiring pure plug flow must operate at high gas velocities (U_0 > approximately (U_{tr} + 1) m/s) and high solids circulation rate (G > approximately 200 kg/m^2 s). If back-mixing is required, as in gas/solid reactors, operation at high enough velocities (U_0 > approximately (U_{tr} + 1) m/s) but at lower values of solids circulation rate (G < approximately 150 kg/m^2 s) is recommended and the operating mode can be described by the core/annulus approach [18,20].

When the gas passes through the bottom zone, some of the particles are entrained with the gas to the upper zone. A part of these entrained particles becomes decelerated and return back to the bottom zone which is caused by the effect of particles bouncing against the top of the riser, while the rest of particles are accelerated to the fully developed zone (the base of the upper zone is called the acceleration zone). Pugsley and Berruti [3] showed that the acceleration effects are also significant in the acceleration zone and it is imperative that solids acceleration effects be considered in the modeling of the axial flow structure. Gungor and Eskin [16] detailed 2D hydrodynamic model demonstrated that at the bottom of the upper zone, in the core region, the acceleration pressure drop component of the total pressure drop changes from 0.65 to 0.28% from the riser center to the core–annulus interface, respectively. The same study also indicates that within the annulus region, the acceleration component of the total pressure drop changes from 0.22 to 0.11% radially from the core–annulus interface to the riser wall. Weinstein and Li [25] estimated the contribution of the particle acceleration component of pressure drop along the acceleration zone to be as much as 40%.

Gungor and Eskin [16] show that even though presented literature models satisfactorily predict the pressure drop in the fully developed zone of the riser, comparison of both models using the cluster-based approach (CBA) (which considers all the solids is moving as clusters) [13,14] and using the particle-based approach (PBA) (which considers the motion of single particles through fluids) [3,9,16] and experimental data show some discrepancies on the pressure drop profile in the acceleration region.

This situation is caused by the fact that the solids are accelerated to an upward velocity, and there is a very large voidage gradient at the base of the upper zone. Therefore, the pressure drop changes considerably within a very short distance. The pressure fluctuations due to the highly turbulent flow in this region also contribute to the poor predictions of the model for transient behavior. Another reason of the deviation could be the fact that the correlations employed in the model for evaluating the voidage have not been adequate for the acceleration zone especially at high solids circulation fluxes. These are the main reasons why both PBA and CBA seem to fail in the precise explanation of the hydrodynamics of the acceleration zone.

With respect to reactions, heat transfer and solid handling in the CFBs, the acceleration zone is of particular importance. The reasons are the relatively higher solids holdup and its strong variation along this zone when compared with the fully developed zone. The hydrodynamics of the acceleration zone is a subject to be studied in more detail and the development of a more accurate model for defining the hydrodynamics of the acceleration zone seems to be extremely important both for research and applications.

It has also been found that the contribution of gas and solids friction components is negligibly small when compared to the acceleration and solids hydrodynamic head components of the total pressure drop [16].

Predicting the axial pressure profile along the riser is one of the major difficulties in modeling the CFB. This profile is an important characteristic of the CFB and a key parameter in its design. An accurate model is needed to predict the pressure profiles. In this study, a model using PBA is developed to accurately predict the axial pressure drop profile especially in the acceleration zone of CFBs. The simulation model takes into account the axial and radial distribution of voidage and the velocity for gas and solid phase, and the solids volume fraction and particle size distribution for the solid phase. The model results are compared with and validated against atmospheric cold CFB experimental literature data [1–3,8,10,14]. Ranges of experimental data used in comparisons are as follows: bed diameter from 0.05 to 0.305 m, bed height between 5 and 15.45 m, mean particle diameter from 76 to 812 μm, particle density from 189 to 2600 kg/m^3, solid circulation fluxes from 10.03 to 489 kg/m^2 s and gas superficial velocities from 2.71 to 10.68 m/s.

2. Model description

The model of this paper uses PBA which considers the two-dimensional motion of single particles through fluids. According to the axial solid volume concentration profile, the riser is axially divided into the bottom zone and the upper zone.

The results of studies of Leckner et al. [26] and Montat and Maggio [27] imply that the particles' mixing and heat transfer in the bottom zone dominate the performance of a CFB for the combustion of coal. On the other hand, it is not clear whether the bed is behaving as a bubbling fluidized bed or is in the turbulent fluidization regime. Schlichthaerle and Werther [7] concluded that in the core region turbulent fluidization is more probable whereas the wall region is rather a dense bubbling fluidized bed. Werther and Wein [28] described the expansion behavior of the turbulent CFB bottom zone by a model that is based on modified equations which were originally developed for conventional bubbling fluidized beds.

In the present model, the bottom zone in turbulent fluidization regime is modeled as two-phase flow which is subdivided into a solid-free bubble phase and a solid-laden emulsion phase. The bubble rise velocity, the bubble volume fraction and the suspension porosity are calculated by Horio [29] as follows:

$$\varepsilon_b = \frac{\dot{V}_b}{u_b} \tag{1}$$

$$\dot{V}_b = \varphi(U_0 - U_{mf}) \quad (\varphi = 1.45Ar^{-0.18}, 10^2 < Ar < 10^4) \tag{2}$$

$$u_b = \dot{V}_b + \gamma\sqrt{gD_b} \tag{3}$$

$$\frac{\gamma}{0.71} = \begin{cases} 0.63 & (D < 0.1\,\text{m}) \\ 2.0\sqrt{D} & (0.1\,\text{m} < D \le 1.0\,\text{m}) \\ 2.0 & (1.0\,\text{m} < D) \end{cases} \tag{4}$$

where D_b is the bubble diameter [30] and U_{mf} is the minimum fluidization velocity [31]. The structure and details of the bottom zone are given in the previous study [16].

The upper zone is located between the bottom zone and the riser exit. The upper zone is assumed to be axially composed of three zones: (i) the acceleration zone is at the bottom part of the upper region, (ii) the fully developed zone is located above the acceleration zone, where the flow characteristics are invariant with height, (iii) the deceleration zone is located above the fully developed zone, where the solids are decelerated depending on the exit geometry of the riser. For the upper zone, the core–annulus flow structure is used [10]. The particles move upward in the core and downward in the annulus. Werther and Wein [28] proposed a correlation which is further confirmed by data from large-scale CFBs. This correlation is used for the calculation of the thickness of the annulus along the riser height.

The model adopts the following simple expressions for the axial profile of the solid fraction along the upper zone. This expression is equivalent to Zenz and Weil [32], and further confirmed by Wein [33] and Bai and Kato [34] for $U_0 = 0.8$–9 m/s, $G = 4$–220 kg/m^2 s, $d_p = 49$–280 μm, $\rho = 706$–4510 kg/m^3.

$$\frac{\varepsilon - \varepsilon_{mf}}{1 - \varepsilon} = \exp[\alpha(h - h_{bot})] \tag{5}$$

where α, the decay coefficient, is a parameter to express the exponential decrease of the solid flux or solid fraction with the height and determined by the following relationship fitted by Cheng and Xiaolong [35] with experimental data:

$$\alpha d_p = 3.8 \times 10^{-5}\left(\frac{G_\infty}{U_0\rho}\right)^{-0.96}\left(\frac{U_0}{\sqrt{gD}}\right)^{-0.84}\left(\frac{\rho - C}{\rho}\right)^{0.37} \tag{6}$$

Eq. (6) reflects the relationship between the decay coefficient, gas/solid properties, flow parameters and particle size. The rate of elutriation above transfer disengaging height, G_∞, is calculated in the model as follows [36]:

$$G_\infty = 0.046 \times C(U_0 - U_t)Re^{0.3}\frac{U_0 - U_t}{\sqrt{gd_p}}\left(\frac{\rho - C}{\rho}\right)^{0.15} \tag{7}$$

where $Re = \rho \times U_0 \times D/\mu$ and ρ is the particle density. It must be noted that Eqs. (1)–(7) should be used to initiate the flow field in the computational domain.

To calculate the cross-sectional average solids concentration, the relationship suggested by Rhodes et al. [37] is used in the model as:

$$\frac{\varepsilon_p}{\bar{\varepsilon}_p} = 1 - \frac{\beta'}{2} + \beta'\left(\frac{r}{R}\right)^2 \tag{8}$$

where the value of β' falls in the range $1.3 \le \beta' \le 1.9$. The solids used in the experimental data of Rhodes et al. [37] are FCC catalyst of mean diameter 74.9 μm and particle density of 2456 kg/m^3 in a bed of diameter ranging from 0.15 to 0.30 m, solid circulation fluxes ranging from 2 to 111 kg/m^2 s and gas superficial velocities ranging from 3 to 5 m/s. β' value is taken as 1.845 in the model calculations.

Table 1
The conservation of mass and momentum equations and the constitutive relations used in this study

Gas phase	Solid phase
Continuity equation	
$\frac{\partial(C\varepsilon)}{\partial t} + \frac{\partial(Cu\varepsilon)}{\partial r} + \frac{\partial(Cu\varepsilon)}{\partial z} = 0$	$\frac{\partial(\rho\varepsilon_p)}{\partial t} + \frac{\partial(\rho v\varepsilon_p)}{\partial r} + \frac{\partial(\rho v\varepsilon_p)}{\partial z} = 0$
Momentum equation	
$\frac{\partial(Cu\varepsilon)}{\partial t} + \frac{\partial(Cu\varepsilon u)}{\partial r} = -\frac{\partial(P\varepsilon)}{\partial r} - \frac{\partial(\tau_{rr}\varepsilon)}{\partial r} - \frac{\partial(\tau_{rz}\varepsilon)}{\partial z} - \beta(u-v)$	$\frac{\partial(\rho v\varepsilon_p)}{\partial t} + \frac{\partial(\rho v\varepsilon_p v)}{\partial r} = -\frac{\partial(\tau_{rr}\varepsilon_p)}{\partial r} - \frac{\partial(\tau_{rz}\varepsilon_p)}{\partial z} + \beta(u-v) - \frac{\partial(G(\varepsilon)\varepsilon_p)}{\partial r}$
$\frac{\partial(Cu\varepsilon)}{\partial t} + \frac{\partial(Cu\varepsilon u)}{\partial z} = -\frac{\partial(P\varepsilon)}{\partial z} - \frac{\partial(\tau_{zz}\varepsilon)}{\partial z} - \frac{\partial(\tau_{zr}\varepsilon)}{\partial r} - \beta(u-v)$	$\frac{\partial(\rho v\varepsilon_p)}{\partial t} + \frac{\partial(\rho v\varepsilon_p v)}{\partial z} = -\frac{\partial(\tau_{zz}\varepsilon_p)}{\partial z} - \frac{\partial(\tau_{zr}\varepsilon_p)}{\partial r} + \beta(u-v) - \frac{\partial(G(\varepsilon)\varepsilon_p)}{\partial z} + \rho g\varepsilon_p$
$\tau_{rr} = 2\mu\frac{\partial u}{\partial r} - \frac{2}{3}\mu\left(\frac{\partial u}{\partial r} + \frac{\partial u}{\partial z}\right)$	$\tau_{rr} = 2\mu_p\frac{\partial v}{\partial r} - \frac{2}{3}\mu_p\left(\frac{\partial v}{\partial r} + \frac{\partial v}{\partial z}\right)$
$\tau_{zz} = 2\mu\frac{\partial u}{\partial z} - \frac{2}{3}\mu\left(\frac{\partial u}{\partial z} + \frac{\partial u}{\partial r}\right)$	$\tau_{zz} = 2\mu_p\frac{\partial v}{\partial z} - \frac{2}{3}\mu_p\left(\frac{\partial v}{\partial z} + \frac{\partial v}{\partial r}\right)$
$\tau_{rz} = \tau_{zr} = \mu\left(\frac{\partial u}{\partial z} + \frac{\partial u}{\partial r}\right)$	$\tau_{rz} = \tau_{zr} = \mu_p\left(\frac{\partial v}{\partial z} + \frac{\partial v}{\partial r}\right)$
Ideal gas equation: $C = \frac{MW_{air}}{R_u}\frac{P}{T}$; $MW_{air} = 28.85\,kg/kmol$	Solids stress modulus [41]; $G(\varepsilon) = \frac{\partial\tau}{\partial(1-\varepsilon)} = 10^{-8.76\varepsilon+5.43}$
	Solid-phase shear viscosity [41]; $\mu_p = \frac{5}{96}\rho d_p\sqrt{\pi T}$
Gas–solid friction coefficient [42]; $\beta = \frac{3}{4}C_D\frac{C\varepsilon(1-\varepsilon)}{\varepsilon^{2.65}}\frac{1}{d_p}\lvert u-v\rvert$	$C_D = \frac{24}{Re_p}(1+0.15Re_p^{0.687})$; $Re_p < 1000$
	$C_D = 0.44$; $Re_p \geq 1000$

In a conventional fluidized bed, the pressure drop through the bed is just equal to the weight of the solids in the bed. Pugsley and Berruti [3] stated that the total pressure drop per unit length along the riser is assumed to be comprised of four main components:

$$\left(\frac{dP}{dz}\right)_{total} = \left(\frac{dP}{dz}\right)_s + \left(\frac{dP}{dz}\right)_{acc} + \left(\frac{dP}{dz}\right)_{fs} + \left(\frac{dP}{dz}\right)_{fg} \quad (9)$$

where $(dP/dz)_s$ is the pressure drop due to the hydrodynamic head of solids, $(dP/dz)_{acc}$ is the pressure drop due to solids acceleration and $(dP/dz)_{fs}$ and $(dP/dz)_{fg}$ are the pressure drops due to solids and gas frictions, respectively.

The pressure drop through the bottom zone is equal to the weight of the solids in this region and considered only in axial direction. Again in the upper zone, the pressure drop, in the axial direction due to the hydrodynamic head of solids is considered while pressure drop due to the solids acceleration is considered in axial and radial directions, the model calculates the acceleration component of pressure drop as follows:

$$\nabla P_{acc} = \frac{1}{2}\rho\nabla(v^2\varepsilon_p) \quad (10)$$

The solids friction and the gas friction components of the pressure drop are considered in the model as boundary conditions in momentum equations for the solid and gas phases, respectively. The solids friction is defined as the frictional force between the solids and the wall, while the gas friction is the frictional force between the gas and the wall.

The properties and the size distribution of particles have significant influence on the hydrodynamics, hence the model also considers the particle size distribution and the attrition phenomena. The particles in the bottom zone include particles coming from the solid feed and recirculated particles from the separator. The particles are discritized into 10 groups. The Sauter mean diameter is adopted as the average particle size.

In the model, it is considered that the particles undergo attrition while moving in the riser. In the fluidized beds, particle attrition takes place by surface abrasion, i.e. particles of a much smaller break away from the original particle. The created particles are fine with a mean diameter of 0.05–0.1 mm or smaller. The upper limit size of the fines produced is in the range of 50–100 μm [38,39]. Weight fraction of particles after attrition is considered as follows:

$$x_a = \frac{k_a(u-v)}{d_{pi}} \quad (11)$$

where k_a is the attrition constant and is obtained varying in the range 2 to 7×10^{-7} [40]. The attrition constant value is taken as 2×10^{-7} in both bottom zone and upper zone in the model. The particles are considered to be spherical. The gas phase is modeled as only flowing upward, backmixing of gas is neglected. The conservation of mass and momentum equations and the constitutive relations used in the model are given in Table 1.

3. Numerical solution

Realistic numerical simulations prove very helpful for the analysis of CFB. Some of the most sophisticated models are based on an advanced computational technique that integrates the discrete element (or particle) method (DEM [43] or DPM [44]) for the solid phase with a CFD algorithm for the fluid phase [14]. Such an approach makes available a series of powerful tools, not available with classical techniques, capable of predicting the core–annulus flow structure, etc. The positions and velocities are calculated for each particle in the system from the forces acting on that particle through integration of Newton's second law of motion and a CFD algorithm (i.e. finite volume approach to solve the continuity and momentum balance equations) is implemented for solving the pressure, velocity, density and voidage fields throughout the system.

The set of differential equations governing mass and momentum for the gas and solid phases are solved using an IBM-PC-AMD processor (CPU speed is 2800 MHz) with a computer code developed by the author [45] in FORTRAN language where the time step is 10^{-6} s. In these equations, the dependent variables are the vertical and the horizontal components of the solid volume fraction, the gas pressure, the gas concentration, the vertical and the horizontal velocity components of the gas and solids. The void fraction is calculated for all control volumes. The

governing continuity and momentum equations for gas and solid phases at each region given in previous study [16], are used in the iterative calculation of the velocity profiles through the calculation domain simultaneously at each time step. The Gauss–Seidel iteration method is used for solution procedure which contains successful relaxation method. The backward-difference method is used the discretization of the governing equations. Flow chart of the numerical solution of the model is shown in Fig. 1.

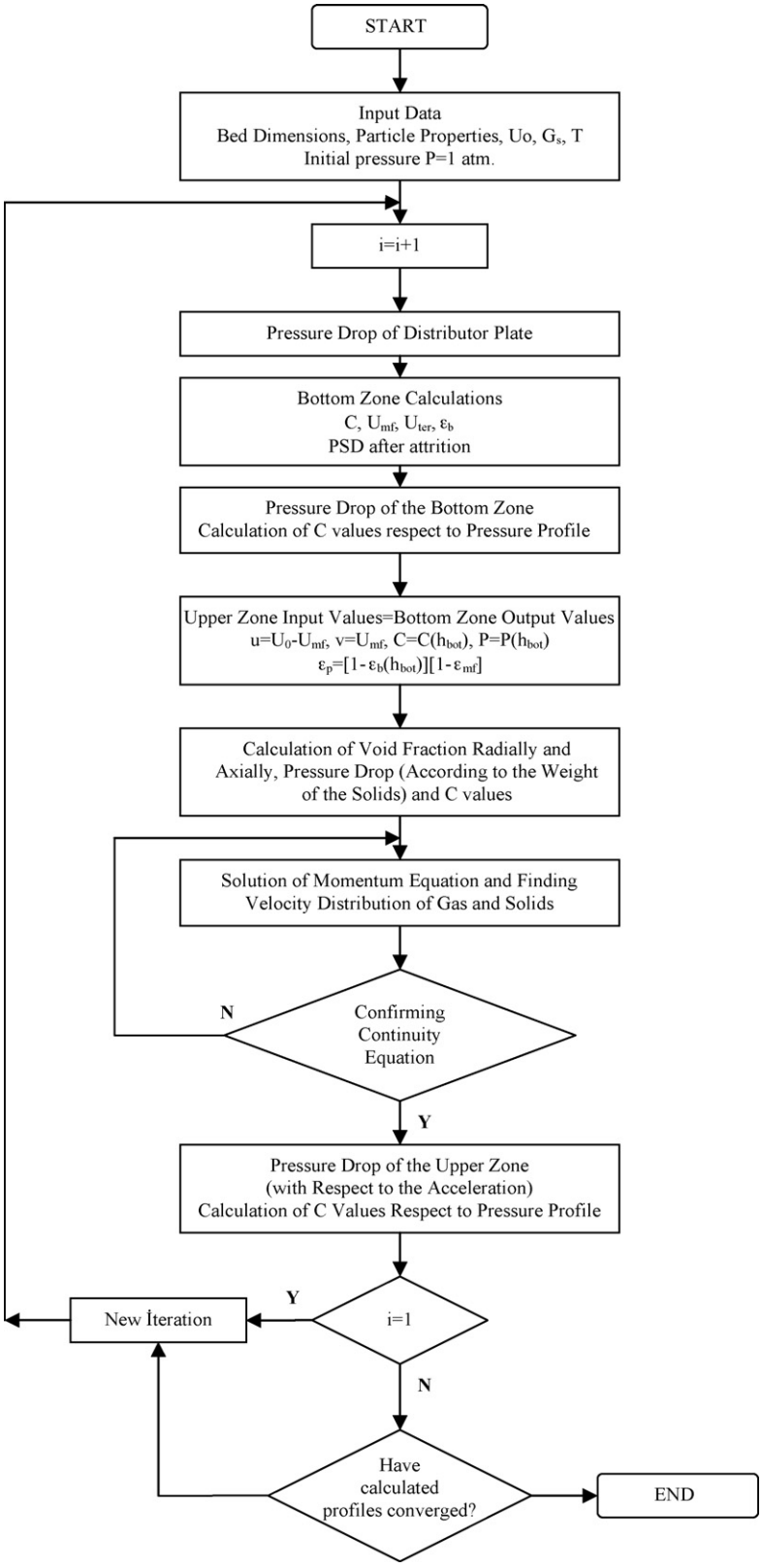

Fig. 1. Flow chart of the numerical solution of the CFB model.

Table 2
Measurement conditions of the experimental data referred to in this study

Author(s)	Particle type	Bed temperature T (°C)	Bed diameter D (m)	Bed height H (m)	Superficial velocity U_0 (m/s)	Particle diamete d_p (μm)	Particle density ρ (kg/m^3)	Solid circulation flux G (kg/m^2 s)
Bader et al. [1]	FCC	25	0.305	12.2	9.1	76	1714	147
	Sand	25	0.2	14.2	4.2	120	2600	50
Knowlton [2]	Sand	25	0.2	14.2	4	175	2145	29
	Sand	25	0.2	14.2	5.8	175	2145	29
Pugsley and Berruti [3]	Sand	25	0.05	5	8.5	208	2580	51.3
	Sand	25	0.05	5	8.5	208	2580	240
Benyahia et al. [8]	FCC	25	0.2	14.2	5.2	76	1712	489
Smolders and Baeyens [10]	Sand	25	0.1	6.47	2.71	90	2600	11.1
Huang et al. [14]	Cork	25	0.305	15.45	9.1	812	189	12.67
	Cork	25	0.305	15.45	10.68	812	189	10.03

The model allows dividing the calculation domain into $m \times n$ control volumes, in the radial and the axial directions and in the core and the annulus regions, respectively. In this study the calculation domain is divided into 10×100 control volumes in the radial and the axial directions and in the core and the annulus regions, respectively. With the cylindrical system of coordinates, a symmetry boundary condition is assumed at the column axis.

In this study, there are boundaries consisting of wall boundaries and an inflow boundary in the computational space domain. At the walls, a partial slip condition is assumed for the solid and the gas phases. Modified Hagen–Poiseuille expression is used for wall friction factor of the gas phase and Konno's correlation is used for the wall friction factor of the solid phase [16].

In terms of the dependent variables in governing equations, the pressure, the void fraction, the particle size distribution, and the superficial velocity are assigned at the inlet boundary in the bottom zone. Other input variables are the bed geometry and the physical properties of gas and solids. No particles are allowed to leave the CFB system. A continuity condition is used for the gas phase at the top of the cyclone. The cyclone is considered as having 100% collection efficiency. In the model, recirculated particles from the cyclone are included to the solid feed particles. Both gas and solid phases are considered isothermal at 298.15 K.

The non-uniform radial distribution of the local particles' axial velocity is a major flow character in the risers. In the riser, the overall radial structure in terms of the particle velocity also shows a core–annulus style where the particles move faster in the core, slower in the annulus with the highest velocity at the centre. Normally, the local particle velocity decreases monotonically from the centre toward the wall. Because of the large amount of downflowing particles in a region adjacent to the wall, the local particle velocity in this region could be negative under certain operating conditions, which causes internal circulation of particles. In the model, it is assumed that the particles move upward axially and move from core to the annulus region radially. Because of assuming a partial slip condition for the solid phase, the particle velocity is determined according to the results of the momentum equation for the tangential direction along the wall surface.

4. Results and discussion

In order to determine the validity of the developed model in terms of axial pressure drop profile along the CFB riser, the simulation results are compared with test results using the same input variables in the tests as the simulation program input [1–3,8,10,14]. The measurement conditions of the experimental data used for the comparison of CFB model are shown in Table 2. The classification of the experimental results in the (U_0, G)-dependent mode of the riser flow is given in Table 3. The transport velocity of particles is determined by the equation of Bi and Grace [24] which is recently verified by the experimental study of Van de Velden et al. [20] as;

$$Re_{tr} = \frac{d_p U_{tr} \rho_g}{\mu} = 1.53 Ar^{0.50} \quad (12)$$

Figs. 2 and 3 show the time-averaged axial pressure drop in the riser compared with experimental data for conditions of Table 2. Generally, the change in the pressure gradient with height in CFB riser is small. In the riser, the pressure gradient is always negative because the gas phase losses pressure head to accelerate and to suspend the particles. The absolute values of the pressure gradient decrease monotonically with increasing distance from the riser entrance and then gradually approach a constant value as clearly shown in Figs. 2 and 3. In the model, calculation of total pressure drop also considers the pressure drop due to distributor plate at the primary gas entrance in the bottom zone. The high pressure drop at the bottom zone is due to the effect of solid feeding in that zone as clearly seen from Fig. 2b and c. The pressure drop then decreased along the height of the riser due to the decrease in solid concentration. The solid lines are in fair agreement with experimental data of Figs. 2 and 3.

The parity plots of predicted pressure drop from the proposed model against the experimental pressure drop are also included for each figure. It could be concluded from these plots that the data points obtained based on the present model are distributed evenly around and close to the parity line which illustrates the fair agreement between the proposed model predictions and the experimental data.

Table 3
The classification of experimental results in the (U_0, G)-dependent mode of riser flow

Author(s)	Particle type	Superficial velocity U_0 (m/s)	Transport velocity U_{tr} (m/s)	Solid circulation flux G (kg/m^2 s)	Flow regime
Bader et al. [1]	FCC	9.1	1.705	147	Regime of core/annulus (mixing) flow
Knowlton [2]	Sand	4.2	2.638	50	Regime of core/annulus (mixing) flow
	Sand	4	2.894	29	Regime of core/annulus (mixing) flow
	Sand	5.8	2.894	29	Regime of core/annulus (mixing) flow
Pugsley and Berruti [3]	Sand	8.5	3.460	51.3	Regime of core/annulus (mixing) flow
	Sand	8.5	3.460	240	Regime of dominant core (plug) flow
Benyahia et al. [8]	FCC	5.2	1.704	489	Regime of dominant core (plug) flow
Smolders and Baeyens [10]	Sand	2.71	2.285	11.1	Regime of core/annulus (mixing) flow
Huang et al. [14]	Cork	9.1	1.846	12.67	Regime of core/annulus (mixing) flow
	Cork	10.68	1.846	10.03	Regime of core/annulus (mixing) flow

Comparisons of simulation results with experimental ones are shown in Fig. 4 for the axial pressure profile along the bed height at two different solids mass flux values: 51.3 and 240 kg/m^2 s. There is a great difference in the axial pressure profiles in the acceleration regions between the plots for the different solids mass flux values. This discrepancy can be explained by the dominant effect of pressure drop due to the acceleration in this region where the difference between the particle and the gas velocities is high. This situation is caused by the fact that in the bottom of the riser the solids are accelerated to an upward velocity, and there is a very large voidage gradient in that area. Therefore, the pressure drop changes greatly within a very short distance. Increasing the solids mass flux causes higher pressure drop in the acceleration region if other parameters are kept unchanged. As a general comment for Fig. 4, it is observed that the increase in the pressure drop is mainly caused by the increase of the hold

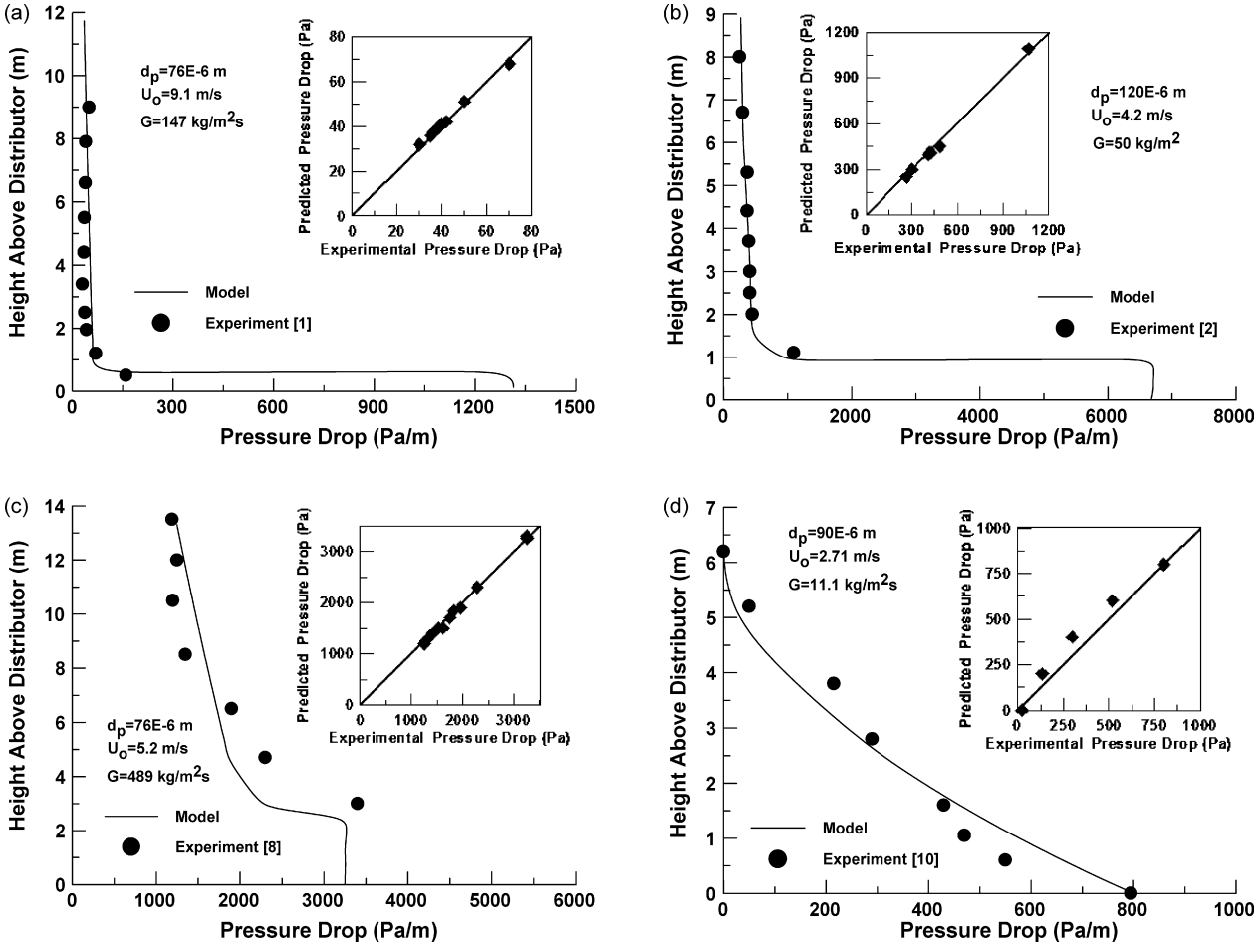

Fig. 2. Comparison of model predictions with: (a) Bader et al. [1], (b) Knowlton [2], (c) Benyahia et al. [8] and (d) Smolders and Baeyens [10] experimental data.

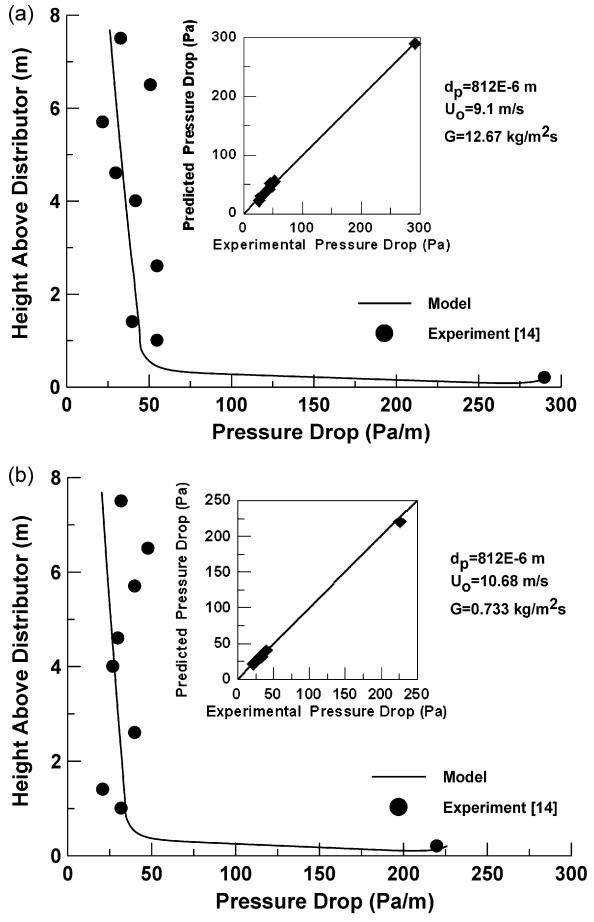

Fig. 3. Comparison of model predictions with Huang et al. [14] experimental data.

up. Fig. 4 also shows that at high solids flux, acceleration zone becomes larger. At these solids mass flux values, the simulations show the same trend as the experiments both in form and magnitude and this accordance shows the model flexibility. This figure also indicates that the model which uses the PBA predicts satisfactorily well at the acceleration zone.

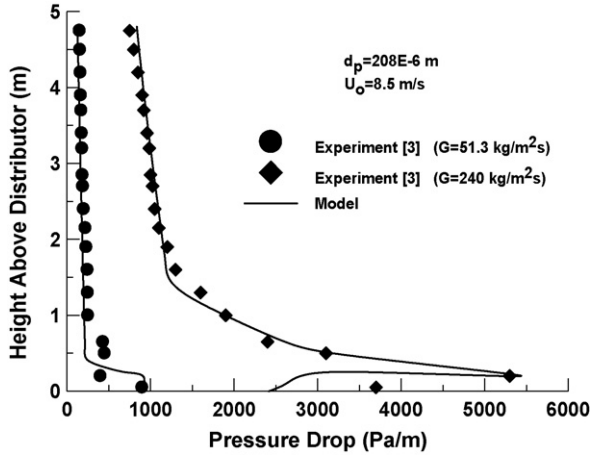

Fig. 4. Comparison of model pressure drop profiles along the bed height with Pugsley and Berruti [3] experimental data for different solids mass flux values.

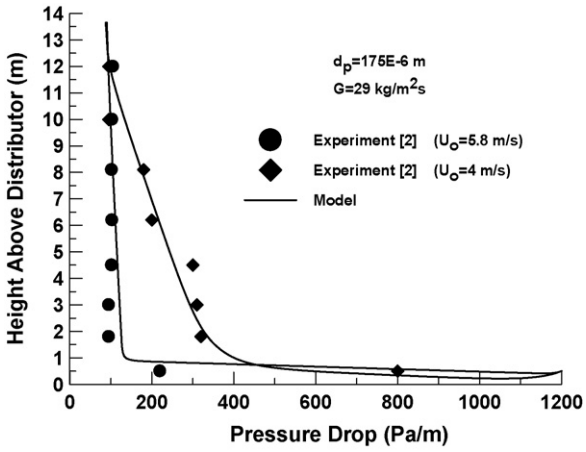

Fig. 5. Comparison of model pressure drop profiles along the bed height with Knowlton [2] experimental data for different superficial velocity values.

The simulations are performed with different superficial gas velocities: 4 and 5.8 m/s at different axial locations (Fig. 5). As the figure displays, the numerical results are in good agreement with the experiments, both in form and magnitude. As it is observed from Fig. 5, variation in the superficial velocity, does affect the acceleration region height. This phenomenon is also observed in the studies of Sabbaghan et al. [13]. Fig. 5 clearly shows that as the superficial velocity decreases, the net solids flux increases and this situation causes higher pressure drop in the acceleration region if other parameters are kept unchanged.

5. Conclusions

In this study, a model using PBA is developed to accurately predict axial pressure drop profile in CFBs. The model results are compared with and validated against atmospheric cold CFB experimental literature data [1–3,8,10,14]. As a result of this study, both the experimental data and the model predictions show that the pressure drop profile is affected by the different solid circulation flux and the superficial velocity values in the riser. The pressure drop has an increasing trend along the acceleration region as the solid circulation flux increases and the superficial velocity decreases in this region.

References

[1] R. Bader, J. Findlay, T.M. Knowlton, Gas/solid flow patterns in a 30.5 cm diameter circulating fluidized bed, in: Proceedings of the 2nd International Circulating Fluidized Bed Conference, Compiegne, France, March 14–18, 1988.
[2] T.M. Knowlton, Modelling benchmark exercise, in: Workshop at the 8th Engineering Foundation Conference on Fluidization, Tours, France, 1995.
[3] T. Pugsley, F. Berruti, A predictive hydrodynamic model for circulating fluidized bed risers, Powder Technol. 89 (1996) 57–69.
[4] A. Svensson, F. Johnsson, B. Leckner, Bottom bed regimes in a circulating fluidized bed boiler, Int. J. Multiphase Flow 22 (1996) 1187–1204.
[5] M.J. Rhodes, M. Sollaart, X.S. Wang, Flow structure in a fast fluid bed, Powder Technol. 99 (1998) 201–209.

[6] H. Lei, M. Horio, A comprehensive pressure balance model of circulating fluidized beds, J. Chem. Eng. Jpn. 31 (1) (1998) 83–94.
[7] P. Schlichthaerle, J. Werther, Axial pressure profiles and solids concentration distributions in the CFB bottom zone, Chem. Eng. Sci. 54 (1999) 5485–5493.
[8] S. Benyahia, H. Arastoopour, T.M. Knowlton, H. Massah, Simulation of particles and gas flow behavior in the riser section of a circulating fluidized bed using the kinetic theory approach for the particulate phase, Powder Technol. 112 (2000) 24–33.
[9] V. Mathiesen, T. Solberg, B.H. Hjertager, Predictions of gas/particle flow with an Eulerian model including a realistic particle size distribution, Powder Technol. 112 (2000) 34–45.
[10] K. Smolders, J. Baeyens, Hydrodynamic modelling of the axial density profile in the riser of a low-density circulating fluidized bed, Can. J. Chem. Eng. 79 (2001) 422–429.
[11] L.C. Gomez, F.E. Milioli, Numerical study on the influence of various physical parameters over the gas–solid two-phase flow in the 2D riser of a circulating fluidized bed, Powder Technol. 132 (2003) 216–225.
[12] L. Huilin, D. Gidaspow, Hydrodynamics of binary fluidization in a riser: CFD simulation using two granular temperatures, Chem. Eng. Sci. 58 (2003) 3777–3792.
[13] H. Sabbaghan, R. Sotudeh-Gharebagh, N. Mostoufi, Modeling the acceleration zone in the riser of circulating fluidized beds, Powder Technol. 142 (2004) 129–135.
[14] Y. Huang, R. Turton, J. Park, P. Famouri, E.J. Boyle, Dynamic model of the riser in circulating fluidized bed, Powder Technol. 163 (1/2) (2006) 23–31.
[15] E. Grieco, L. Marmo, Predicting the pressure drop across the solids flow rate control device of a circulating fluidized bed, Powder Technol. 161 (2006) 89–97.
[16] A. Gungor, N. Eskin, Hydrodynamic modeling of a circulating fluidized bed, Powder Technol. 172 (2007) 1–13.
[17] J. Yerushalmi, N.T. Cankurt, D. Geldart, B. Liss, Flow regimes vertical gas–solid contact systems, AIChE Symp. Ser. 176 (74) (1978) 1–13.
[18] M. Van de Velden, J. Baeyens, K. Smolders, Solids mixing in the riser of a circulating fluidized bed, Chem. Eng. Sci. 62 (2007) 2139–2153.
[19] K. Smolders, J. Baeyens, Overall solids movement and solids residence time distribution in a CFB-riser, Chem. Eng. Sci. 55 (2000) 4101–4116.
[20] M. Van de Velden, J. Baeyens, J.P.K. Seville, X. Fan, The solids flow in the riser of a circulating fluidised bed (CFB) viewed by positron emission particle tracking (PEPT), Powder Technol. 183 (2008) 290–296.
[21] Y. Molodtsof, Theoretical analysis of the flow regimes and their characteristics in vertically flowing gas–solids suspensions, Chem. Eng. J. 96 (2003) 133–143.
[22] E.R. Monazam, L.J. Shadle, J.S. Mei, J. Spenik, Identification and characteristics of different flow regimes in a circulating fluidized bed, Powder Technol. 155 (2005) 17–25.
[23] S. Bhusarapu, M. Al-Dahhan, M.P. Dudukovic, Quantification of solids flow in a gas–solid riser: single radioactive particle tracking, Chem. Eng. Sci. 59 (2004) 5381–5386.
[24] H.T. Bi, J.R. Grace, Flow regime diagrams for gas–solid fluidization and upward transport, Int. J. Multiphase Flow 21 (1995) 1229–1236.
[25] H. Weinstein, J. Li, An evaluation of the actual density in the acceleration section of vertical risers, Powder Technol. 57 (1) (1989) 77–79.
[26] B. Leckner, M.R. Golriz, W. Zhang, B.A. Andersson, F. Johnsson, Boundary layers-first measurements in the 12 MW CFB research plant at Chalmers University, in: Proceedings of the 11th International Conference on Fluidized Bed Combustion, ASME, 1991, pp. 771–776.
[27] D. Montat, T.D. Maggio, 1D two-phase description of the thermal hydraulic behavior of the furnace of E. Huchet 125 MWe CFB boiler, in: Proceedings of 5th International Conference CFB, MSR6, Beijing, 1996.
[28] J. Werther, J. Wein, Expansion behavior of gas fluidized beds in the turbulent regime, AIChE Symp. Ser. 301 (90) (1994) 31–44.
[29] J.R. Grace, A.A. Avidan, T.M. Knowlton, Circulating Fluidized Beds, Blackie Academic & Professional, London, 1992.
[30] S. Mori, C.Y. Wen, Estimation of bubble diameter in gaseous fluidized beds, AIChE J. 21 (1975) 109–117.
[31] C.Y. Wen, Y.H. Yu, Mechanics of fluidization, Chem. Eng. Prog. Symp. Ser. 62 (1966) 100–110.
[32] F.A. Zenz, N.A. Weil, A theoretical–empirical approach to the mechanism of particle entrainment from fluidized beds, AIChE J. 4 (1958) 472–479.
[33] J.W. Wein, Das expansionsverhalten von gas/feststoff-wirbelschicten bei hoheren gasgeschwindigkeiten, Ph.D. Thesis, TU Hamburg-Harburg, Germany, 1992.
[34] D.R. Bai, K. Kato, Generalized correlations of solid holdups at dense and dilute regions of circulating fluidized beds, in: Proceedings of 7th SCEJ Symposium CFB, Society of Chemical Engineering, Tokyo, Japan, 1994, pp. 137–144.
[35] Y. Chen, G. Xiaolong, Dynamic modeling and simulation of a 410 t/h pyroflow CFB boiler, Comp. Chem. Eng. 31 (2006) 21–31.
[36] I. Tanaka, H. Shinohara, H. Hirasue, Y. Tanaka, Elutriation of fines from fluidized bed, J. Chem. Eng. Jpn. 5 (1972) 51–57.
[37] M.J. Rhodes, X.S. Wang, H. Cheng, T. Hirama, Similar profiles of solids flux in circulating fluidized bed risers, Chem. Eng. Sci. 47 (7) (1992) 1635–1643.
[38] Q. Wang, Z. Luo, X. Li, M. Fang, M. Ni, K. Cen, A mathematical model for a circulating fluidized bed (CFB) boiler, Energy 24 (1999) 633–653.
[39] M.J. Rhodes, D. Geldart, The upward flow of gas/solid suspensions. Part 2. A practical quantitive flow regime diagram for the upward flow of gas/solid suspensions, Chem. Eng. Res. Des. 67 (1989) 30–37.
[40] Q. Wang, Z. Luo, M. Ni, K. Cen, Particle population balance model for a circulating fluidized bed boiler, Chem. Eng. J. 93 (2003) 121–133.
[41] W. Wang, Y. Li, Hydrodynamics simulation of fluidization by using a modified kinetic theory, Ind. Eng. Chem. Res. 40 (2001) 5066–5073.
[42] C.Y. Wen, Y.H. Yu, Mechanics of fluidization, Chem. Eng. Progr. Symp. Ser. 62 (1966) 100–110.
[43] D. Rong, M. Horio, DEM simulation of char combustion in a fluidized bed, in: Proceedings of 2nd International Conference CFD in the Mineral and Process Industries, Melbourne, Australia, December 6–8, 1999.
[44] J. Li, J.A.M. Kuipers, Effect of pressure on gas–solid flow behavior in dense gas-fluidized beds: a discrete particle simulation study, Powder Technol. 127 (2002) 173–184.
[45] A. Gungor, Modeling of circulating fluidized bed combustors, Ph.D. Thesis, Istanbul Technical University, Turkey, 2006.